PROCEEDINGS, 50th Workshop on Geothermal Reservoir Engineering
Stanford University, Stanford, California, February 10-12, 2025
SGP-TR-229

Critical Fracturing Considerations for Enhanced Geothermal Systems

Ludmila Belyakova[1], and Abdul Muqtadir Khan[1]

[1]SLB, Sugar Land

Corresponding Author: Akhan813@slb.com

Keywords: Enhanced Geothermal Systems, Hydraulic Fracture Optimization, Proppant Transport Modeling, Thermoelastic Stress Effects, FORGE

ABSTRACT

Analyzing the success of recent enhanced geothermal systems (EGS) projects such as the Frontier Observatory for Research in Geothermal Energy (FORGE), Red and Cape Stations, key findings such as circulation rate dependence on the size of the stimulated volume and networks are evident. This paper proposes some optimization aspects at the scale of each fracture and completion scheme at large. Four aspects are modeled and explored:

1. High Temperatures and Proppant Transport: High temperatures lead to lower viscosities and significantly accentuates proppant settling and sand duning; hence, the transport of lightweight proppant is considered.
2. Polylactic Acid-Based Degradable Fiber: The use of polylactic acid-based degradable fiber in proppant slurry can lower friction pressure and enhance proppant transport. Both these aspects are critical for uniform fracture conductivity and effective heat exchange. These processes have been modeled using a novel multiphysics particle-in-cell slurry flow model, which tracks mass loss-based degradation and digitized material profiles.
3. Thermoelastic Stress Alterations: The impact of thermoelastic stress alterations during fracturing has been given less importance due to the fracturing fluid cooling down the temperature transient. A conceptual model, issues related to accurately scaling up this physics in numerical models, and the criticality of embedding these effects in the fracturing phase for EGS models is discussed .
4. Other considerations: Other critical considerations such as the proppant demobilization impact, geochemical processes coupling framework, choice of proppant, etc. have been discussed.

All numerical modeling is conducted on a calibrated FORGE stress and leakoff model with accurate structural dip. The considerations are expected to provide multiple answers for various optimization phases in the recent future of EGS, not just in hot-dry-rock scenarios but also in slightly permeable basement rock scenarios such as the eastern part of North America and Asia. Cost analysis for optimization has also been presented where required.

1. INTRODUCTION

Enhanced Geothermal Systems (EGS) represent a significant advancement in sustainable energy development, offering a reliable and scalable technology for extracting geothermal heat and harnessing the power production capacity from hot rock formations. Fracturing is the backbone of EGS development, and a lot can be learned from oil and gas industry which has seen the evolution of conventional an unconventional fracturing at scale. However, the geothermal prospects present a challenging environment in terms of deeper, hotter rock with different geology. Moreover, the circulation and production phases that follow fracturing posit more hurdles which require careful consideration for successful deployment. This paper intends to explore few key optimization considerations, providing a broad perspective, and setting the stage for detailed upcoming work by the authors in these areas. We particularly focus on proppant transport, thermal stress effects, and proppant demobilization.

Proppant transport has been investigated with the use of light weight proppant and polylactic acid-based degradable fibers. Fibers have been very effective for many applications over decades. Khan et al. (2023a) have shown that through morphology and chemistry optimization fibers provide wide array of functionalities related to bridging, plugging, particle suspension, and scrubbing/cleaning actions. Across completions and production engineering workflows, these actions can branch into multiple specific applications, one of them being enhanced proppant transport. At conceptual level, among other things, we also discuss (a) the thermoelastic effect on fracture propagation during fracturing which has received less attention; (b) proppant demobilization through the EGS project lifespan.

All the simulations performed for this investigation were on the FORGE dataset, and conducted in the novel, state of the art, Multiphysics (MP) hydrodynamics numerical model developed by Isaev et al. (2023) and Velikanov et al. (2018). The authors there propose a novel Lagrangian numerical model for simulating slurry flow in hydraulic fractures, with a focus on proppant transport and settling. The goal is to improve the accuracy of slurry dynamics using a hybrid Eulerian-Lagrangian approach, which enhances tracking of proppant movement while addressing computational inefficiencies in traditional models. The model is based on lubrication theory, describing the movement of fluid and proppant in narrow fractures and utilizes nonlinear hyperbolic equations to represent slurry dynamics. The Eulerian approach is used for flux discretization and initial condition setup. The Lagrangian approach is employed for tracking proppant transport along velocity fields. Adaptive seeding/reseeding strategies ensure computational efficiency while maintaining accuracy. This approach has many strengths such as (a) eliminating excessive numerical diffusion compared to fully Eulerian methods, improving resolution of sharp

concentration fronts. (b) preserving volume conservation while providing precise tracking of slurry components. (c) computational efficiency is significantly improved through localized time-step refinement and adaptive particle seeding. (d) better handling of non-uniform injection profiles allows for modeling pulsed fracturing treatments. The model primarily developed for channel fracturing (with pulsed slurry steps) and accurate multi-material modeling (Khan et al. 2022). Most other fracturing simulators based on Eulerian approach are not capable of representing proppant pulses due to excessive numerical diffusion and coarse grids The proppant transport model captures the gravitational and hindered settling components and is consistent among all commercial models (detailed and explained in Isaev et al. 2023).

The experimental degradation data for different degradable products based on their temperature range were digitized in the numerical simulator. The fiber degradation is then simulated as a function of exposure time spent at the transient temperature during injection. A hindered settling factor, ranging from 0 to 1, where 0 implies strong effect of fibers on settling, is calculated based on the fiber quality. This sequence allows accurate calculation of the proppant concentration based on the slurry transport. This sequence is presented through an output of a simulator in Figure 1. The dependence of hindered settling factor on fiber degradation metric obtained experimentally by Badazhkov and Plyashkevich (2018) is digitized into the software for calculations.

The critical considerations for EGS which have been well documented in the literature have not been discussed here. These include, (a) updated laboratory testing to understand elastic and other material properties evolution with temperature and stress cycling; (b) the need for utilization proppant; (c) importance of modeling the conductivity and injectivity enhancement due to shear induced fractures.

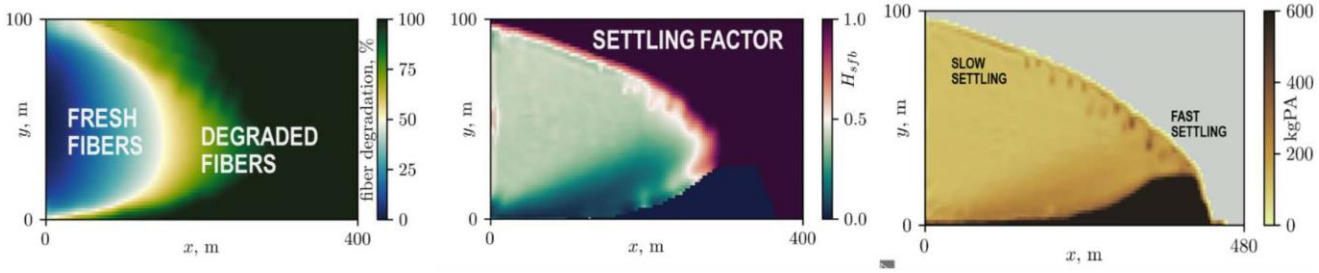

Figure 1: Simulation of degradable fibers conducted in the numerical model: (left) output showing the degradation percentage of fibers across the fracture cross-section; (center) hindered settling factor calculation as a function of fiber degradation; (right) proppant concentration resulting as a consequence of faster settling due to fiber degradation. (modified from Idimeshev et al. 2021)

2. EGS CHALLENGES AND CONSIDERATIONS

High temperatures of geothermal reservoirs may potentially lead to several placement issues. One of the challenges is maintaining fluids' viscosity: low viscosity, even if successfully placed, leads to excessive proppant settling and consequently, sub-optimal proppant distribution. In order to evaluate this process and prevent undesirable consequences, we performed a sensitivity study, varying or editing pump schedule parameters. We consider the following parameters: two types of proppant transport aid (light weight proppant, and fiber particles), proppant type, different ratio of standard and light weight proppants, fiber effects on proppant distribution. A study was performed for two fluid viscosities to evaluate it influence on proppant placement and distribution. Appendix 1 summarizes parameters changes and related case names. Some exploration of other critical challenges is also provided in addition to the above sensitivity study.

We consider a single dominant fracture, thus, Multiphysics model with Planar 3D propagation model was used All results are based on well 16A(78)-32, stage 5, perforated with a single cluster at 10020-10026-ftMD, with 36 total shots.

2.1 Proppant transport

2.1.1 Base case 1 description

We consider a conventional pump schedule shown in Table 1 where proppant is injected homogeneously with monotonically increasing concentration. The fluid for all steps is.a crosslinked gel with power law rheology from n'=0.32, k'=2E-5lbf*s^n/ft^2 at 410^{o}F to n=0.32, k=0.287 lbf.s^n/ft2 at 160^{o}F. Injection rate is 35 bbl/min for the whole schedule.

Table 1: Bottomhole pumping schedule for a base case.

Step #	Step name	Proppant type	Prop. Conc., PPA	Proppant mass (lbm)	Slurry vol. (bbl)	Pumping time, min
1	Pad		0.0	0.00	654	18.7
2	0.5 PPA	100 mesh	0.5	12600	614	17.5
3	0.75 PPA	100 mesh	0.75	17986	590	16.9

4	1 PPA	100 mesh	1.0	24108	600	17.1
5	1 PPA	40/70 sand	1.0	23982	597	17.1
6	1.2 PPA	40/70 sand	1.2	26208	548	15.7
7	1.4 PPA	40/70 sand	1.4	29988	542	15.5
Total	-	-	-	134873	4146	118.5

Leakoff coefficient in the simulations corresponding to this base case is set to Ct= 3.1E-4 ft/min$^{0.5}$. Spurt loss is set to 0 m. These parameters were obtained from matching fracture geometry to micro-seismic data.

Formation properties in the fracture initiation zone are shown in Table 2.

Table 2: Formation properties in a fracture initiation zone for a base case.

Property	Average True vertical depth (TVD), ft	Bottomhole static temperature (BHST), F	Reservoir pressure, psi	Closure pressure, psi	Permeability, md	Young's Modulus	Poissin's Ratio
Value	~8,100	410	~3,800	~6,200	1E-06	6.1E+06	0.27

2.1.2 Proppant mesh size

Figure 2 demonstrates proppant distribution for the base case 1 at the end of job (EOJ) and after closure (ACL) moments. Given the impact of higher temperature which heats up the fluid and degrades the crosslink, even though the transport with the crosslink fluid is better, significant proppant settling is observed until fracture closure. For stage 5 in 16A(78)-32, the pressure falloff was monitored for 15 minutes, and it declined about 500-psi. Based on the minimum horizontal stress, the transient pressure during well shutin was still ~1,800 psi above the expected closure, hence the closure time for all the cases was set at 100 minutes.

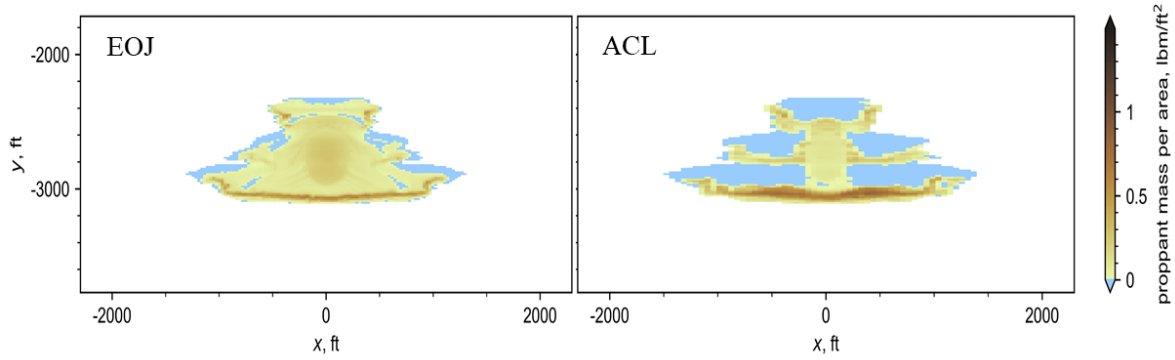

Figure 2: proppant mass per area distribution for the base case 1, end of the job (EOJ) - left, after closure (ACL) – right.

Replacing proppant of the base case 1 from 40/70 to 30/50 (Case 1) leads to more pronounced settling at both the EOJ (higher propped area within the fracture is seen with lower concentrations) and ACL (higher proppant concentration at the fracture bottom) moments (Figure 3).

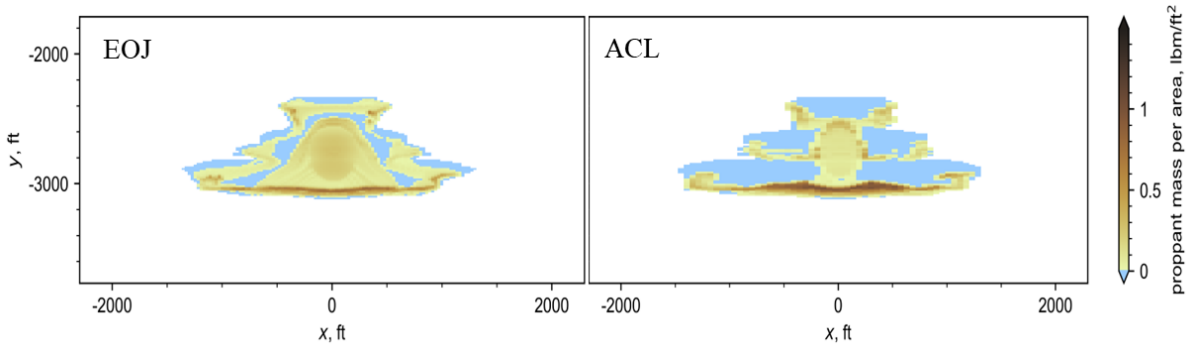

Figure 3: Case 1: proppant mass per area distribution with 30/50 sand, end of the job (EOJ) - left, after closure (ACL) – right.

2.1.3 Fiber influence on proppant distribution

Fibers are added to the proppant slurry for enhanced transport. The addition of fiber to the base fluid enables an increase of effective carrying fluid viscosity, therefore reducing the critical settling velocity for a given proppant type. The fibers dispersed in the fluid interact mechanically with the proppant particles to reduce the settling velocity.

Figure 4 and 5 demonstrates proppant distribution in presence of high temperature (HT) fibers for the base case 1 (Case 2) and Case 1 with 30/50 sand (Case 3). For both cases noticeable improvement of proppant distribution (less settling) is observed at both the end of job (EOJ) and after closure (ACL) moments. Moreover, the near wellbore proppant concentration is higher, which makes it promising for enhancing injection rates. For the case 3, with larger proppant, the proppant settling is higher but better than the smaller proppant without fibers (base case 1).

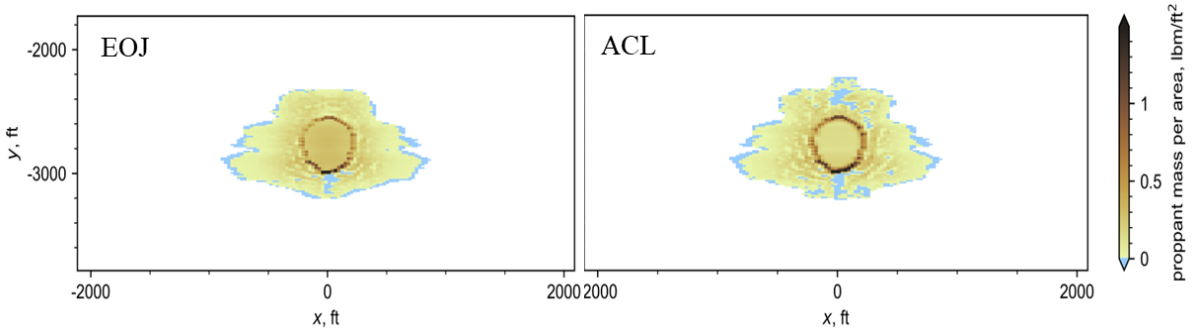

Figure 4: Case 2: proppant mass per area distribution with HT fiber, end of the job (EOJ) - left, after closure (ACL) – right.

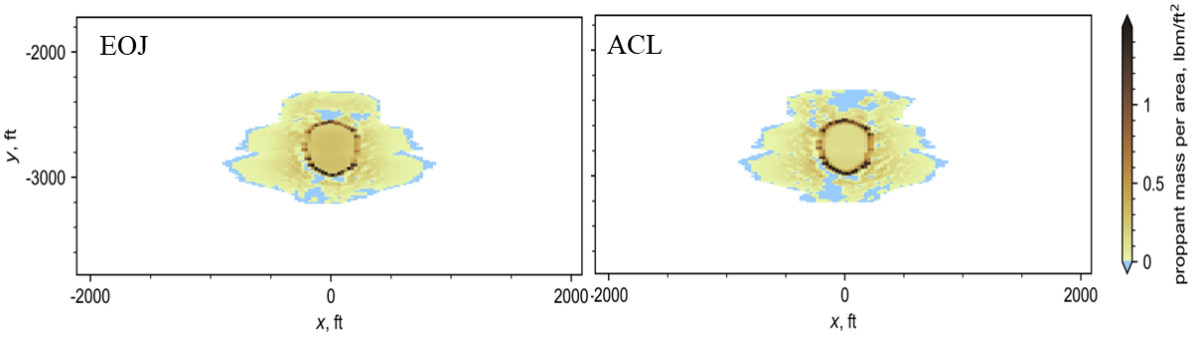

Figure 5: Case 3: proppant mass per area distribution with HT fiber, end of the job (EOJ) - left, after closure (ACL) – right.

Addition of fibers influence not only proppant distribution but also fracture geometry. Fiber enhances proppant distribution across the fracture height as well, thus, leading to less propped length. Figure 6 demonstrates EOJ proppant distribution of the base case 1 (left, no fiber) and case 2 – the base case with HT fibers (right). A note here is that careful optimization of fiber concentration is important because hyper-normal fibers concentration could lead to excessive bridging.

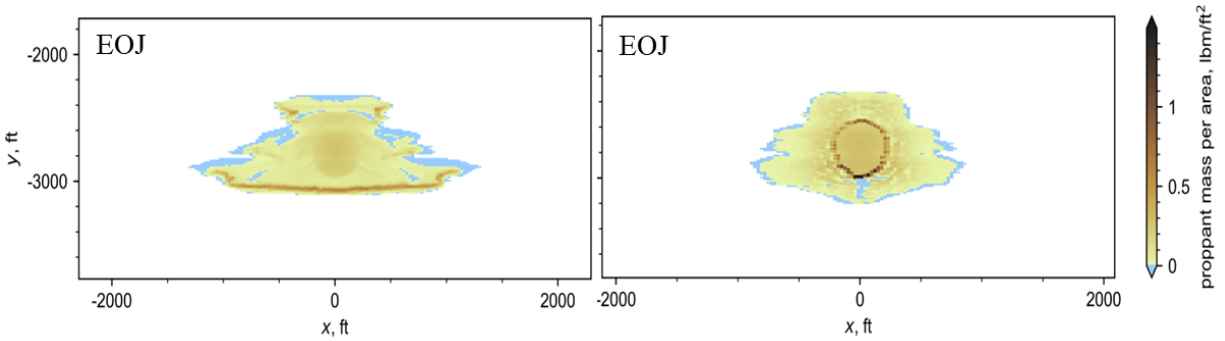

Figure 6: fracture geometry comparison for the base case 1 (left, no fibers) and Case 2 – the base case 1 with HT fibers (right).

2.1.3 Light weight proppant (LWP) influence on proppant distribution

Stage 10 in the well 16A(78)-32 had 4,000-lbs of 30/80 mesh ultra lightweight proppant placed at 0.03 ppg concentration through the treatment (England et al. 2025). The proppant has an SG of 1.066 which can lighten the slurry significantly. We tried to explore the expansion of this transport aid to improve proppant distribution through the fracture. Table 3 summarizes properties of propping agents: conventional and light-weight.

Table 3: Sand properties.

Property	100 mesh	100 mesh_LWP	Sand 40/70	Sand 40/70_LWP
Specific gravity	2,.65	1.07	2.64	1.07
Bulk density, lb/gal (lb/ft3)	12.35 (92.39)	5,59 (41.80)	13,94 (104.25)	5.59 (41.80)

Figure 7 demonstrates after closure proppant distribution for two cases: base case 1 with 100 mesh and Sand 40/70 and Case 4 – base case 1 with both types of sand replaced by the lightweight option. We can clearly see that with light-weight sand distribution significantly improved as less settling is observed.

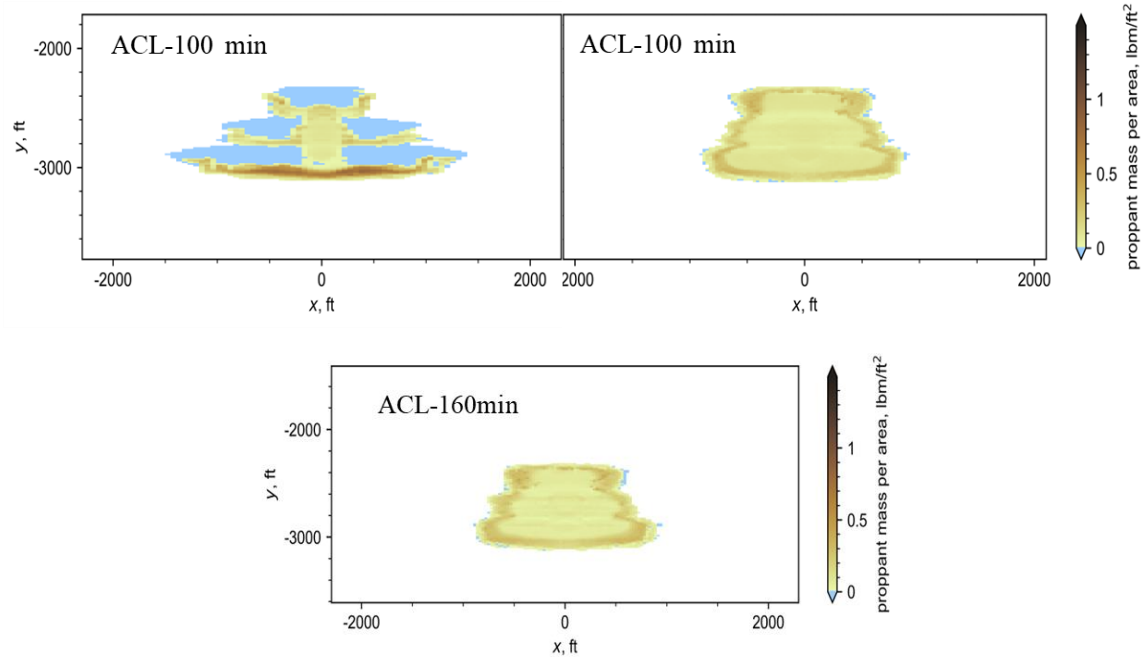

Figure 7: proppant distribution comparison for the base case 1 (top left, conventional sand); Case 4 – the base case 1 with light weight sand with 100 minutes shutin time (top right); Extended shutin case with 160 minutes closure time (bottom)

Another observation is that, similarly to a case with fibers, fracture has become shorter. This mechanism could be explained by proppant being transported to the fracture tip sooner (in the fibers and light weight cases) and altering the transient leakoff at the fracture face. Also, since the weight of proppant is almost similar to the base fluid, the settling rate is almost negligible as observed with the extended shutin plot.

Full sand replacement to the lightweight option may have significant impact on the stage cost and overall project economics. To find a cost-effective solution, where cost and proppant distribution are optimized systematically, we varied mass of light weight sand 40/70 in a pump schedule. Table 4 summarizes proppant type combinations for considered cases. All other parameters of pump schedules were as in the base case 1.

Table 4: Proppant type combinations.

Step #	Step name	Base case 1	Case 5 (~ 30% of total slurry - 40/70 LWP)	Case 6 (~ 63% of total slurry - 40/70 LWP)	Case 4
1	Pad				
2	0.5 PPA	100 mesh	100 mesh_LWP	100 mesh_LWP	100 mesh_LWP
3	0.75 PPA	100 mesh	100 mesh_LWP	100 mesh_LWP	100 mesh_LWP
4	1 PPA	100 mesh	100 mesh_LWP	100 mesh_LWP	100 mesh_LWP
5	1 PPA	40/70 sand	40/70 sand_LWP	40/70 sand_LWP	40/70 sand_LWP
6	1.2 PPA	40/70 sand	40/70 sand	40/70 sand_LWP	40/70 sand_LWP
7	1.4 PPA	40/70 sand	40/70 sand	40/70 sand	40/70 sand_LWP

Figure 8 demonstrates proppant distribution at after closure moment for cases detailed in table 4. We may notice less settling with higher percent of LWP pumped.

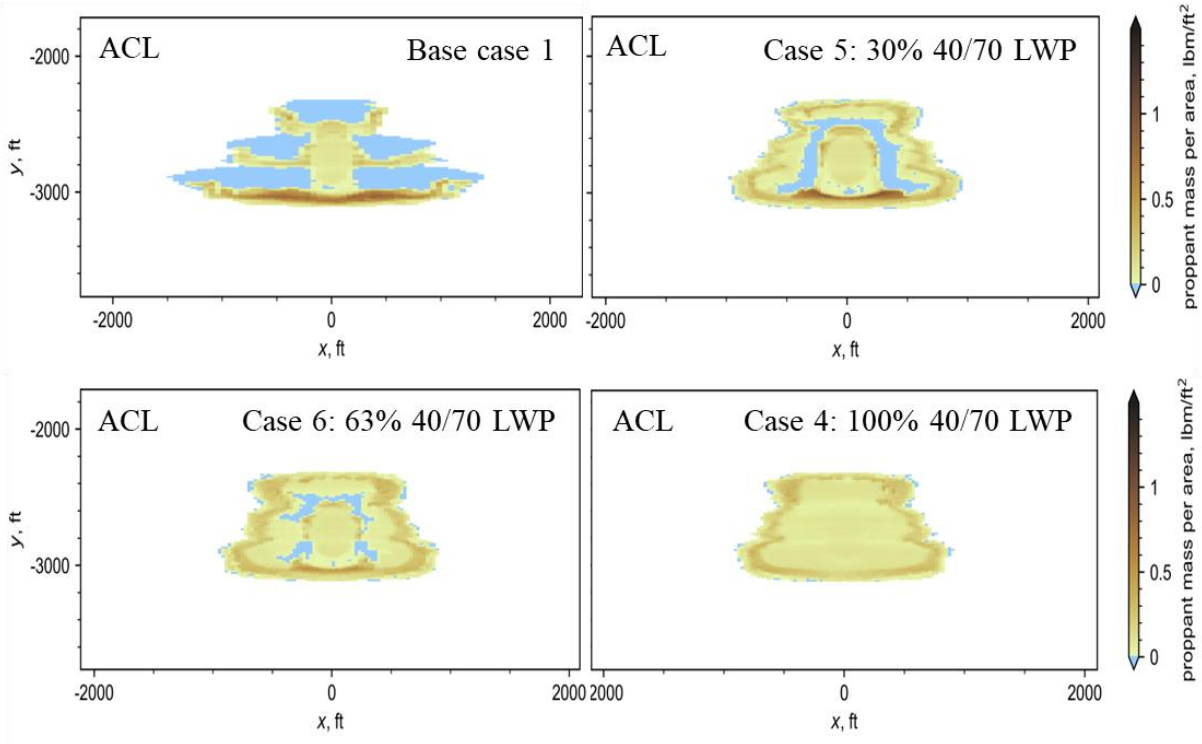

Figure 8: proppant distribution with different mass of sand 40/70 LWP.

To further investigate and optimize proppant distribution in the Case 5 (~30% 40/70 LWP) and in a Case 6 (63% 40/70 LWP), we considered fibers addition. The fibers were added at two different concentrations in the slurry fraction that does not have the LWP. Which

means for Cases 7 and 8, 70% of the slurry has fibers and for Cases 9 and 10, 37% of the slurry has fibers added, Based on case 5 - HT fiber was added to proppant stages with conventional 40/70 sand with lower concentration (Case 7) and higher concentration (Case 8). Figure 9 demonstrates proppant distribution for Cases 7 and 8. It can be observed that higher fiber concentration makes proppant distribution better. Based on Case 6 - HT fiber was added to proppant stages with conventional 40/70 sand with lower concentration (Case 9) and higher concentration (Case 10). Figure 10 demonstrates proppant distribution for Cases 9 and 10. Similarly to the Cases 7 and 8, higher fiber concentration makes proppant distribution better. Compared to the extended shut-in scenario for 100% LWP, some higher settling is seen here for the extended closure time simulations. But, still it is much better with significantly higher times, showing that the hindered settling rate affects better proppant distribution.

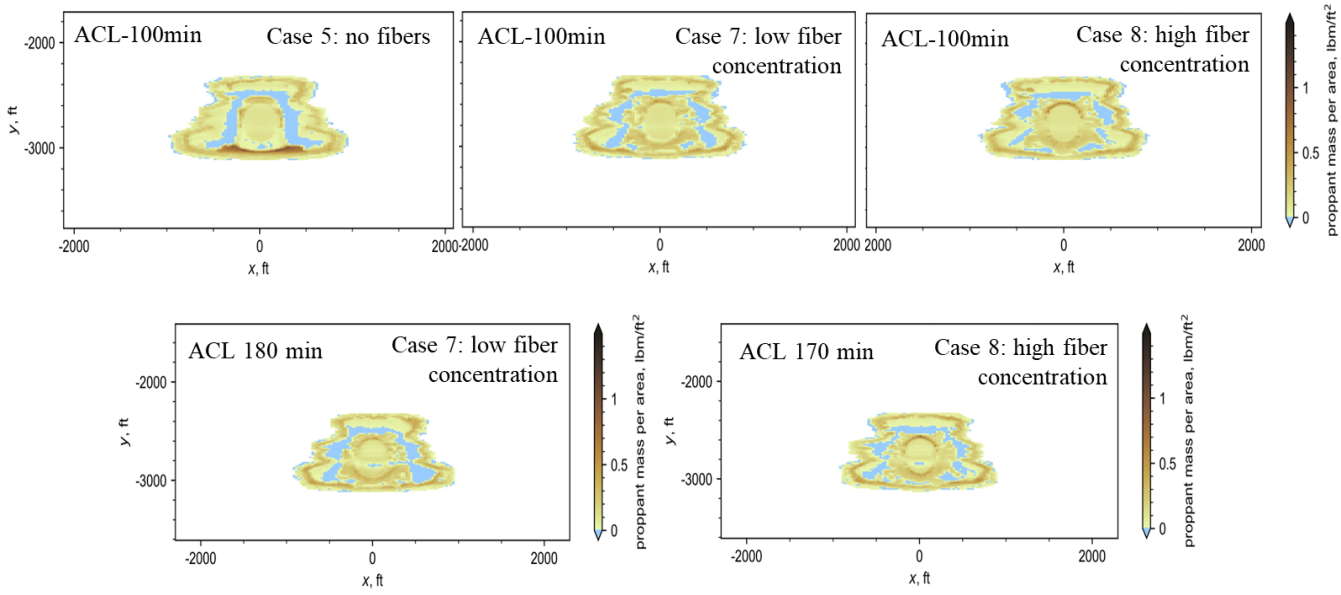

Figure 9: proppant distribution with different HT fiber concentration for the Case 5 (30% sand 40/70 LWP). Bottom row plots show the extended shutin time cases.

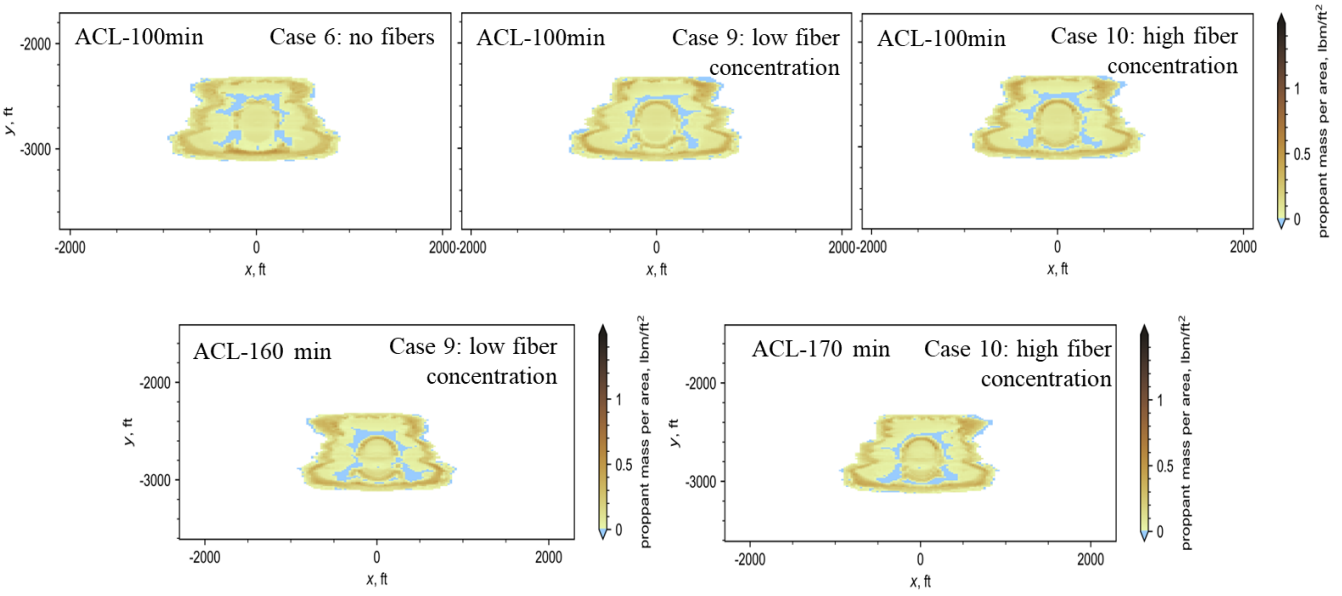

Figure 10: proppant distribution with different HT fiber concentration for the Case 6 (63% sand 40/70 LWP). Bottom row plots show the extended shutin time cases.

2.2 Fluid type considerations

In comparison to the Base case 1 with a crosslinked fluid, we considered a Base case 2 with low viscous fluid (n'=1, k'=2E-5 lbf.s^n/ft^2). Other parameters of a pump schedule are the same as described in a Table 1.

Figure 11 compares proppant distribution for the base case 1 (crosslinked fluid) and base case 2 (low viscous fluid) both cases at after closure (ACL) moment. Predictably, base case 2 fracture is shorter in height, longer and narrower compared to the base case 1. Also, the higher rate for the cluster (i.e., 35-bbl/min) aids in longer fracture generation. Lower fracture width leads to less proppant settling, as fracture closes faster.

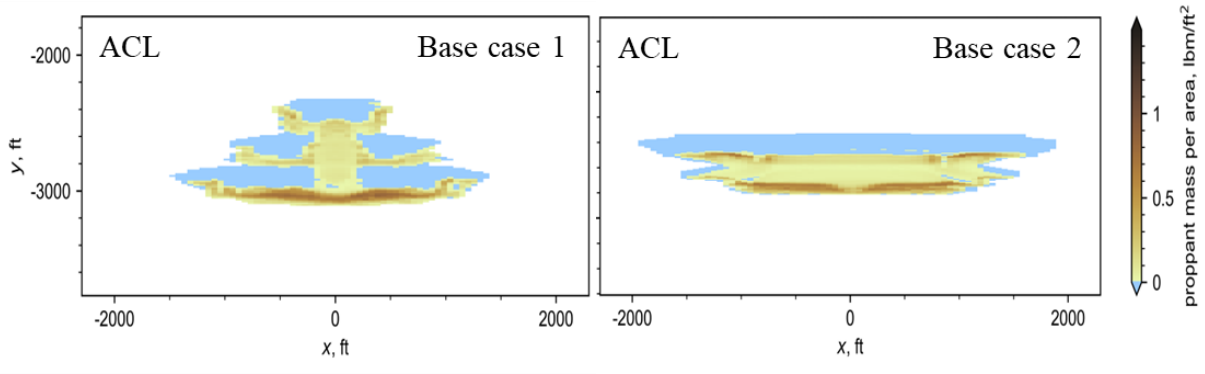

Figure 11: proppant distribution for the base case 1 (crosslinked fluid, left) and the base case 2 (low viscous fluid, right).

Sensitivity study to proppant type, fibers addition, and LWP percentage changes resulted in the same conclusion as for the base case 1. We would like to discuss a pump schedule optimization with LWP and fibers.

Figure 12 demonstrates how fibers addition improves proppant distribution for a Case 11 (low viscous fluid, 30% 40/70 LWP). It is noticeable that both low and high concentrations of HT fiber, added to conventional sand 40/70 steps, significantly improves proppant distribution in narrower fracture, compared to wider fracture, created with a crosslinked gel (Figure 9).

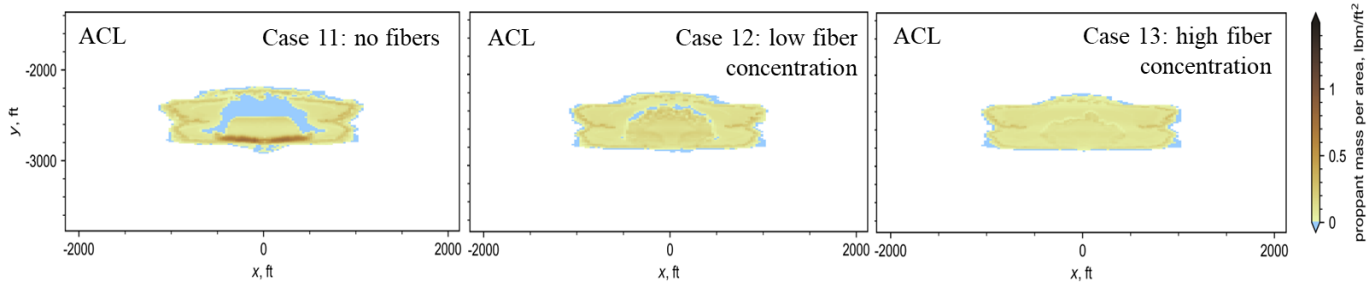

Figure 12: proppant distribution with different HT fiber concentration for the Case 11 (low viscous fluid, 30% sand 40/70 LWP).

Even better results in terms of proppant distribution can be observed with more LWP in a pump schedule. Figure 13 shows proppant distribution for a Case 14 (low viscous fluid, 63% 40/70 LWP) with different HT fiber concentration. It is noticeable that even low fiber concentration significantly improves proppant distribution (Case 15). It should be noted here that fibers addition can complicate proppant placement by causing excessive bridging, thus fibers concentration should be carefully selected.

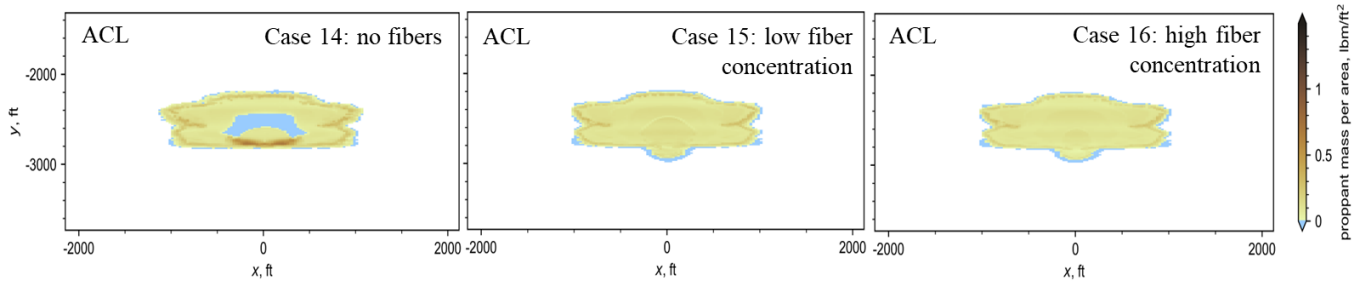

Figure 13: proppant distribution with different HT fiber concentration for the Case 14 (low viscous fluid, 63% sand 40/70 LWP).

Finally, it is important to consider the cost component in the optimization exercise. From the fracture propagation footprints analyzed, we computed the total propped and hydraulic fracture surface areas for each case and tried to utilize that ratio as a cost optimization parameter. Cases with 30% and 63% LWP were compared with the basecase, wherein the other slurry was laden with fiber (70% and 37% respectively). Hence for lower LWP amounts, the cost component is relative higher for fibers. Moreover, the fiber loading itself was sensitized within those cases, which affects the fiber cost. Figure 14 below shows a summary of the above sensitivity where the basecase without any proppant transport aids are used, shows a very low proppant footprint at ~45% area only covered with proppant. The plot clearly shows that increasing investment can optimize the proppant distribution and this analysis can be used in the overall techno-commercial analysis of EGS projects.

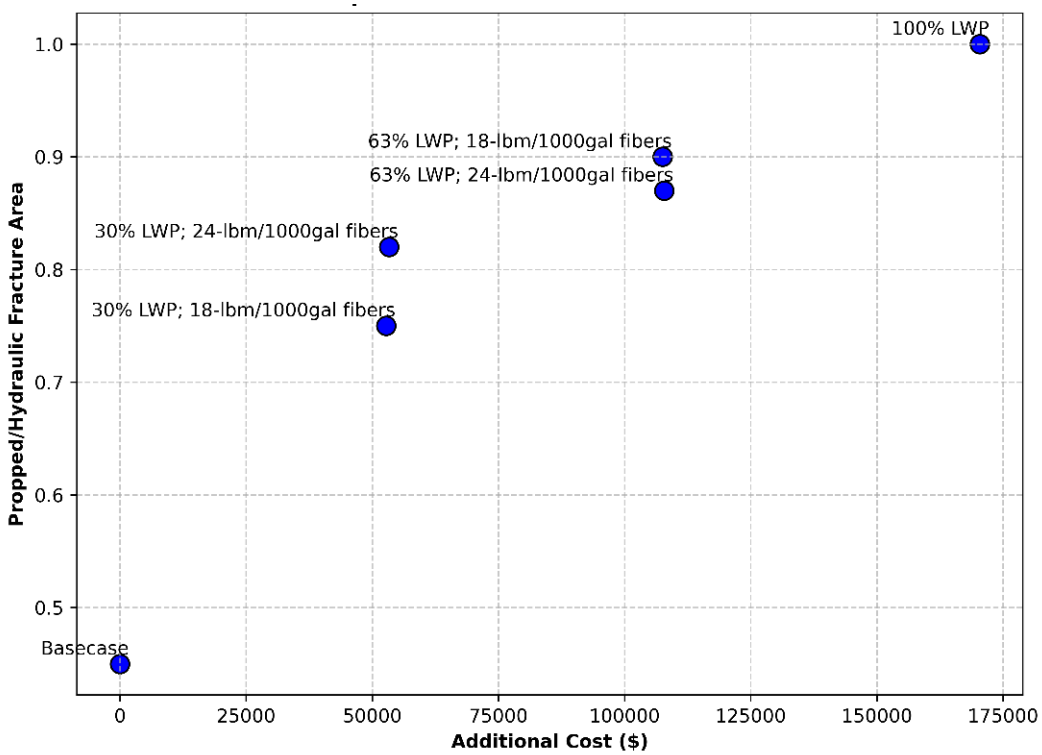

Figure 14: Additional cost versus proppant/hydraulic fracture surface area for optimization of the proppant transport aids' design consideration.

2.3 Thermal effects during fracturing

In the context of EGS thermoelastic stress effect is well established and studied during the circulation and production phase of the project. McClure et al. (2024) have provided a robust forward modeling study using the thermoelastic effect during circulation and long term production at the FORGE project which demonstrated stress changes upto 1,000s of psi, resulting in significant fracture apertures upto 1.5-in. But the consideration in this paper is to question whether this effect should be modeled during fracturing also. The understanding today is that the thermoelastic stress induction during fracturing might not be significant because, once the temperature transient equilibrates with the cooldown temperature, the thermal stress alterations would be minimal for the short time scale (Khan et al. 2024).

In order to explore this, we investigated the cooldown in the fracture through a simple simulation of the stage 5 in the 16A-78(32) well at FORGE. Figure 15 below shows the temperature cooldown in the near wellbore region upto ~200-ft away from the wellbore reaches 94ºC (201^{o}F) which represents a differential cooldown of ~106^{o}C (~210^{o}F) from the initial static temperature.

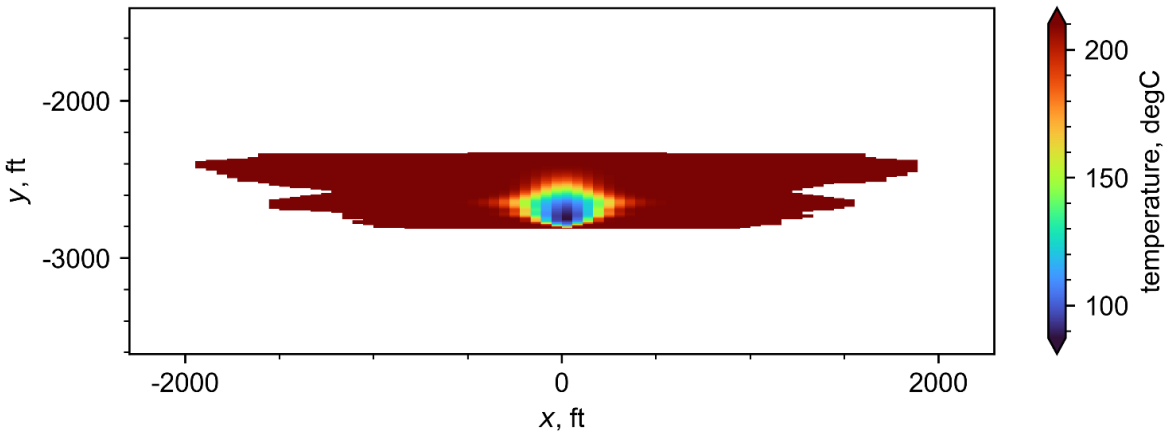

Figure 15: End of fracturing treatment temperature cooldown plot for stage 5 in the 16A-78(32) well showing 106ºC (201ºF) lowest temperature. Horizontal and vertical axis represent fracture length and height dimensions, respectively.

Figure 16 below shows a simplified thermoelastic component effect varying with increasing cooldown. The figure is a simplified visual to study the impact based on the stress equation below.

$$\sigma_T = \sigma_0 - \frac{\alpha E \Delta t (1-\upsilon)}{1-2\upsilon}$$

Where, σ_T is the total stress, σ_0 is the lithostatic stress, α is the thermal expansion coefficient of the rock, E is the elastic Young's Modulus, υ is the Poisson's Ratio, and Δt is the temperature change as a result of the cooldown.

This analysis showed that at a reference initial lithostatic stress of 12,000-psi and a cooldown of 100ºC, the absolute stress reduction will be ~1,800-psi (15% reduction) which is significant in the context of barrier stress and vertical fracture propagation. But it is exaggerated for that consideration. When we consider the effect of cooldown on reduction of breakdown pressure of rock, Figure 16 can be useful but in this scenario, the cooldown is significant in the fracture length and height dimensions but not in the width dimension. With width being in few orders of magnitude lower, the cooldown in the small fracturing treatment timescale of pumping might not affect the bulk rock volume enough to cause an impact.

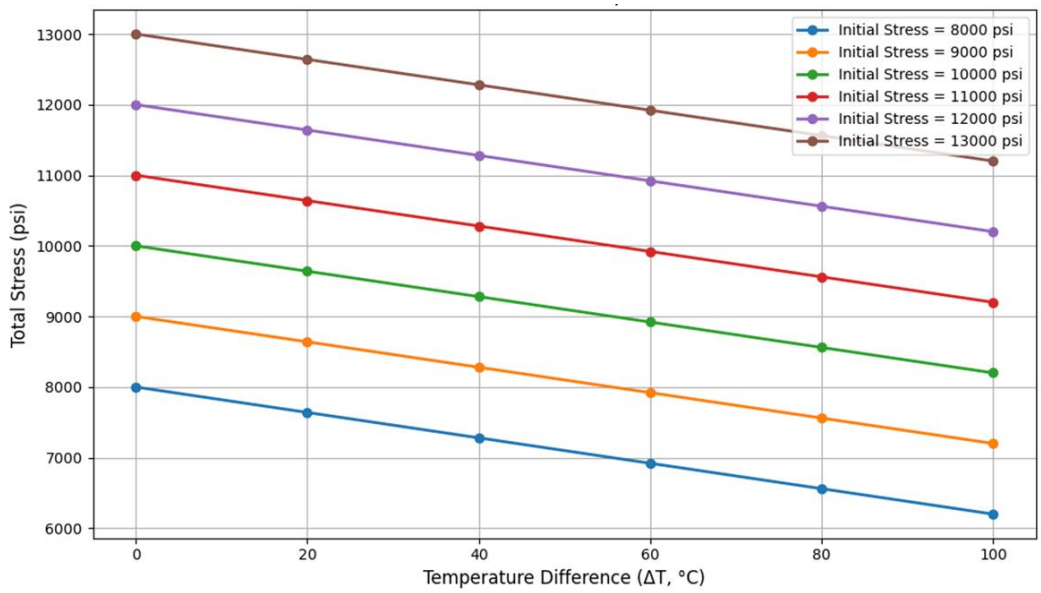

Figure 16: Total stress (including thermal component) versus the temperature difference for varying original stress magnitudes for constant elastic and thermal properties i.e., υ=0.25; E=6E+06 psi; α=2E-06 /ºC.

Further investigation was conducted to study the 3D stress field, and this effect can be observed in Figure 17. A finite difference approximation of the heat diffusion was implemented with the rock properties (thermal conductivity, rock density, specific heat capacity, static temperatures, etc.) from the FORGE dataset and literature on Granitoid properties. The initialization boundary condition was

simplified for the objective by (a) fixing the cooldown to the maximum cooled down temperature (100°C) at time = 0 and studying the diffusion for 50 minutes; (b) rock temperature initially uniform at 210°C.

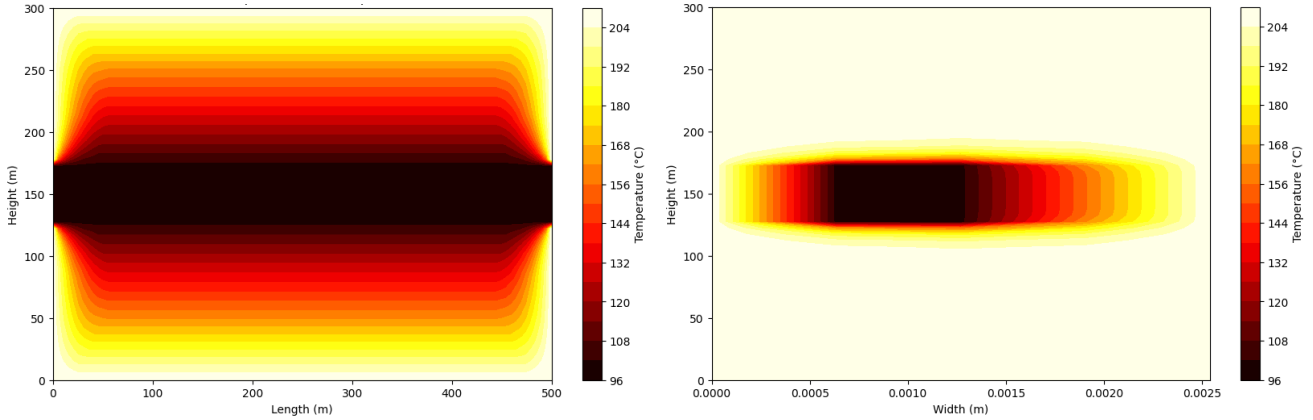

Figure 17: 3D Temperature field: (left) fracture height versus fracture length, (right) fracture height versus fracture width.

This raises two important questions (a) will this cooldown in the width dimension cause a localized stress change at the inch or sub-inch scale and create a pinched downward fracture propagation along the length of the fracture? Or this effect will create a negligible impact on propagation. Even if it is propagated down, it might not be propped (b) how would we implement gridding to account for this modeling? because in regular practice the fracture cells in the 3D grid are of the order of few feet. So there needs to be some technique to scale the temperature in the fracture cells to account for this effect. Alternately, a logarithmically refined grid can be used with the fracture cells at an inch or sub-inch scale. But we know this would be computationally expensive at best and numerically unstable at worst. (c) in context of EGS where high efficiency operations are expected, and the wellbore temperature does not go above 130°C even during shutin (Norbeck et al. 2023), this cooldown in the width dimension might be more than usual from the temperature transients of multiple fractures, considering all fractures are transverse. Hence these considerations require in-depth modeling to assess the impact and effect.

2.4 Proppant Mobilization

In the longer term circulation and production phase, proppant pack mobilization is a critical factor governing the conductivity, mass flow rates, and temperature evolution in EGS projects. Chuprakov et al. (2020) and later Chertov et al. (2021) have presented field validation of recent advanced modeling to simulate the proppant pack mobilization based on digitizing the laboratory results of flow testing. Figure 18 below taken from Khan et al. (2023b) shows an example demonstrating the criticality of the pack destabilization and rearrangement under drawdown conditions. It can be seen that the near-wellbore proppant was produced due to high filtration rates leaving massive unpropped fracture surface area resulting in a low effective conductivity by end of flowback period. This is a severe problem in oil and gas but more so for EGS where continuous injection and production of fluids have higher likelihood of proppant destabilization and changing the conductivity of the network significantly over the timespan of the project. Such coupled modeling solutions or Safe Operating Envelope strategies should be employed for future EGS development.

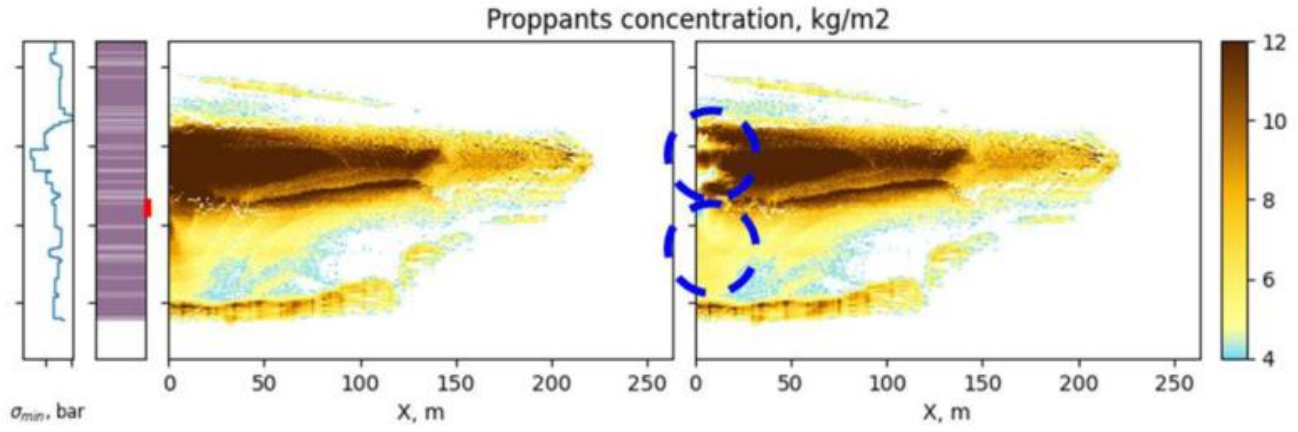

Figure 18: Numerical modeling results to demonstrate proppant pack stability/demobilization in drawdown conditions (Khan et al. 2023b).

2.5 Other critical considerations

2.5.1 Geochemical coupling:

Chemical processes in the subsurface systems (rock, faults, fractures) include scale deposition, rock and proppant dissolution, change of fluid properties because of bulk or surface reactions, etc. The chemical composition of produced fluid can drastically change during the lifespan of the EGS projects (<34 hours, Jones et al., 2023). These rock-fluid-proppant interactions can alter the porosity and permeability of the fracture system generated, leading to modified (reduced) injectivity and transmissivity. A reactive transport model that numerically simulates these chemical processes is needed to predict the chemical and physical evolution of the circulating fluids and associated reservoir damage and prevent or mitigate scaling and corrosion (Figure 19). Kresse et al. (2024) have detailed this requirement in their recent review paper on EGS.

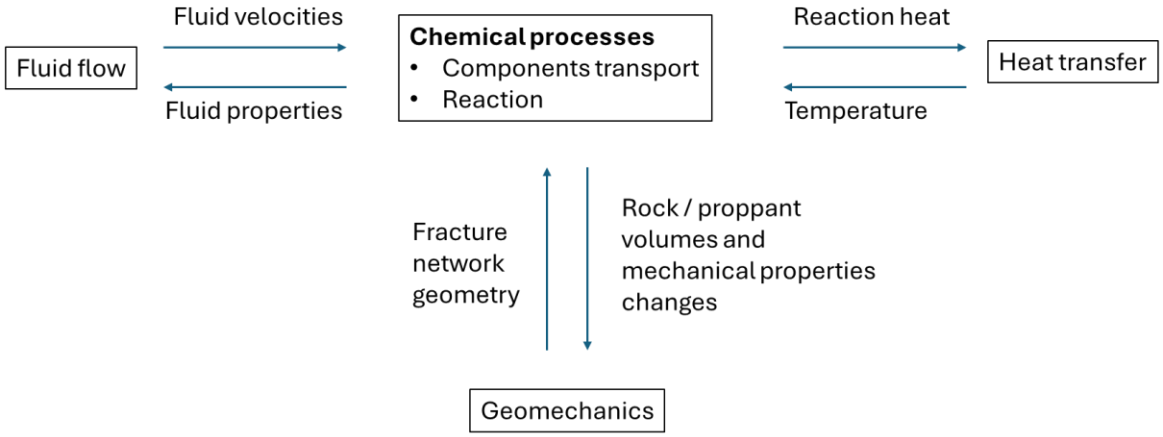

Figure 19: Modeling framework to couple the geochemical processes with fracturing, fluid flow and geomechanics (Kresse et al. 2024)

2.5.2 Choice of proppant:

Unconventional fracturing has optimized economics with sand as the main proppant type and following that practice might be detrimental in long term EGS performance. Sand can have significant dissolution along with silica scales generation and hence higher strength, more robust ceramic proppant (bauxite) should be considered. Development of sophisticated organic chemistry for scale mitigation that does not degrade at high EGS operating temperatures would be very useful as coating material for commercial high strength proppant grades or even optimized for coating sand.

3. DISCUSSION AND WAY FORWARD

Below are few discussion points for the sensitivity study and other concepts explored in this paper:

- This paper intends to provide control experiments to study the effect of different proppant transport aids and hence the discrete natural fracture (DFN) network was not considered here along with the complex model. Even though the simulations conducted here are on planar-3D geomechanical model coupled with the novel multiphysics slurry flow, the recommendation based on observations from FORGE data is that a complex fracture model will be apt for EGS modeling as detailed by Khan et al. (2024)
- The choice for the single cluster stage 5 from the FORGE injector well was due to the same reason of providing a control sensitivity so the differential rate (flux) per cluster does not affect the interpretations. Since this was a single cluster and rate per perforation hole and rate per fracture is higher at 35 bpm/cluster, this could have been the reason for low viscosity system shows better basecase results in terms of proppant distribution.
- Carrying fluids type will be important not only in terms of proppant placement, but also the resulting proppant distribution. More viscous fluids create wider fractures with potentially more settling. Thus, in terms of proppant distribution, when we add fibers or LWP, generally, we observe better results in narrower fractures, created by low viscous fluids.
- Fiber addition improves overall proppant distribution. The fiber concentrations selected for this study were chosen for technology exploration purposes based on the field implementation history. In actual EGS environments, where stiffer rock is expected, concentrations should be selected with consideration of both placement and proppant distribution.
- Utilization of LWP generally gives better results in terms of proppant distribution, compared to cases with just fibers or mixed LWP plus fibers. The enhanced modeling provides an input to the final design decision which must integrate the considerations for placement, injectivity and cost implications.
- Longer closure time versus proppant distribution: The modeling results of proppant distribution discussed in this paper will strongly depend on fracture closure time, which is a function of both reservoir parameters (stresses, leakoff) and created fracture geometry (what do we pump and how do we pump). Some cases were modeled to show the resilient effect of the proppant transport aids presented here but this could change for specific cases. Longer fracture closure time will potentially lead to more settling.

As a way forward, the authors would like to highlight and explore in their future works the following areas:

- Detailed 3D gridded modeling will be conducted to study the effect of thermoelastic stress change on fracture propagation during fracturing.
- A limitation of this study is that the impact of the proposed designs on injectivity and circulation rates has not been evaluated. This was done to limit the discussion to fracture generation, and the assumption was that a better proppant distribution implies a better design and higher injectivity. In EGS context though, injectivity plays a critical role, thus proppant distribution optimization should be evaluated not only in terms of costs, but also in injectivity metrics. This flow modeling will be conducted and detailed in our future papers.
- Proppant demobilization and its effect on injectivity: Even more importantly, fracture injectivity in a long-term perspective should be evaluated. One of parameters to consider is proppant demobilization while circulating fluids. Possible sand movement in a closed fracture may influence fracture injectivity and in a worst case scenario, lead to wellbore disconnection. These effects will also be modeled on the FORGE subsurface model to study the impact on injectivity.

4. CONCLUSIONS

The findings presented in this study highlight the complexities and critical factors involved in optimizing EGS fracturing and completion strategies. The analysis demonstrates that high-temperature conditions which affect the viscosity significantly influence proppant transport and distribution across the hydraulically generated fracture, necessitating innovative solutions such as lightweight proppants and degradable fibers. Additionally, the modeling of thermoelastic stress alterations provides valuable insights into fracture height propagation, reinforcing further research for the need for incorporating these effects into EGS designs which can observe large differential temperatures from the static conditions while fracturing. Moving forward, continued research into proppant mobilization, long-term injectivity, and geochemical coupling will be essential for maximizing EGS efficiency. The proposed study, cost optimizations and recommendations serve as a guide for future developments, contributing to the engineered evolution of geothermal stimulation and enhancing the viability of EGS as a sustainable energy solution.

REFERENCES

Badazhkov, D. and Plyashkevich, V.: Methodology of Fibers Impact Calculation on Proppant Transport in Hydraulic Fracture. SPE-191718-18RPTC-MS. Paper presented at the SPE Russian Petroleum Technology Conference, Moscow, Russia, 15−17 October (2018).

Chertov, M., Salazar S., Franck I., Kaznacheev, M., and Belyakova, L.: Combined Proppant Placement and Early Production Modeling Achieve Increased Fracture Performance in Ecuador's Oriente Basin. SPE-204677-MS. Paper presented at the SPE Middle East Oil & Gas Show and Conference, November (2021).

Chuprakov, D., Belyakova, L., Iuldasheva, A., et al.: Proppant Flowback: Can We Mitigate the Risk? SPE-199748-MS. Paper presented at the SPE Hydraulic Fracturing Technology Conference and Exhibition, The Woodlands, Texas, USA, February (2020).

England, K., Li, P. J., Xing, P., Moore, J. and McLennan, J. 2024 Enhanced Geothermal System Hydraulic Fracturing Campaign at Utah FORGE. Paper presented at the SPE Hydraulic Fracturing Technology Conference and Exhibition, The Woodlands, Texas, USA, February (2025).

Idimeshev, S. V., Isaev, V., Ismailovich, T., Alexandrovich, A., Semin, L. G., Bannikov, D. V., Velikanov, I., Vladimirovich, I., Maxim G., Kuznetsov, D. S., and Belyakova, L.S.: Digital Slot: A Tool for Optimization and Development of New Hydraulic Fracturing Technologies. Paper presented at the SPE Russian Petroleum Technology Conference, Virtual, October (2021).

Isaev, V., Idimeshev, S., Semin, L., and Tikhonov, A.: A Lagrangian Method for Slurry Flow Modeling in Hydraulic Fractures. Geoenergy Science and Engineering, Vol. 231, Part A, (2023).

Jones, C. G., England, K., Simmons, S., Rose, P., Mella, M., Barker, B., McLennan, J., and Moore, J.: Stimulation, Tracers and Geochemistry at Utah FORGE. PROCEEDINGS, 48th Workshop on Geothermal Reservoir Engineering Stanford University, Stanford, California, February 6-8, (2023).

Khan, A., M., Isaev, V., and Belyakova, L.: Multimaterial Multiphysics Modelling Coupled with Post-Fracturing Production Flow Simulations: Revamping Hydraulic Fracturing Design Strategy. Paper presented at the SPE Asia Pacific Oil & Gas Conference and Exhibition, Adelaide, Australia, October (2022).

Khan, A. M., McLennan, J., Kresse, O., England, K., Xing, P., Hobbs, B., and Deville, B.: Integrated Lifecycle Simulation for Utah FORGE: Part I – Fracture Geometry Calibration. GRC Transactions, Volume 48, Hawaii, October (2024).

Khan, A. M., Binziad, A., and Alsubaii, A.: Degradable Chemistry Provides Solutions For Production Enhancement and Intervention in Challenging Wells. SPE-215707-MS. Paper presented at SPE International Hydraulic Fracturing Technology Conference and Exhibition, Muscat, Sultanate of Oman, 12–14 September (2023a).

Khan, A.M., Binziad, A., Alsubaii, A., Glaznev, I., Alekseev, A., Kuznetsov, D.: Proppant Flowback Control in Deep Hot Gas Wells Using Unconventional Proppant. SPE-215626-MS. Paper presented at SPE International Hydraulic Fracturing Technology Conference and Exhibition, Muscat, Sultanate of Oman, 12–14 September (2023b).

Kresse, O., Khan, A. M., Gutierrez-Sosa, L., Hobbs, B., Sosio, G., Emelyanov, D., and Mehay, S.: A Review of Enhanced Geothermal Systems Life Cycle Optimization: Laboratory Experimentation, Material Properties, and Numerical Modeling. GRC Transactions, Volume 48, Hawaii, October (2024).

McClure, M., Irvin, R., England, K., and McLennan, J.: Numerical Modeling of Hydraulic Stimulation and Long-Term Fluid Circulation at the Utah FORGE Project. PROCEEDINGS, 49th Workshop on Geothermal Reservoir Engineering Stanford University, Stanford, California, February 12-14 (2024).

Norbeck, J., Latimer, T., Gradl, C., Agarwal, S., Dadi, S., Fercho, S., Lang, C., McConville, E., Titov, A., Voller, K., and Woitt, M.: A Review of Drilling, Completion, and Stimulation of a Horizontal Geothermal Well System in North-Central Nevada. PROCEEDINGS, 48th Workshop on Geothermal Reservoir Engineering, Stanford, California, February 6-8 (2023).

Velikanov, I., Isaev, V., Bannikov, D., Tikhonov, A., Semin, L., Belyakova, L., and Kunetsov, D.: New Fracture Hydrodynamics and In-Situ Kinetics Model Supports Comprehensive Hydraulic Fracture Simulation. SPE-190760-MS. Paper presented at the SPE Europec featured at 80th EAGE Conference and Exhibition, Copenhagen, Denmark, 11–14 June (2018).

APPENDIX 1

TableA1. Sensitivity study cases description

Case name	Description	Changes made to the base case
Base case 1	Fluid type: crosslinked, sand type: 100 mesh + 40/70	
Case 1	Fluid type: crosslinked, sand type: 100 mesh +30/50	Sand type replaced to 30/50
Case 2	Fluid type: crosslinked, sand type: 100 mesh +40/70+ high temperature (HT) fiber	Base case 1 + HT fiber
Case 3	Fluid type: crosslinked, sand type: 100 mesh +30/50+ high temperature (HT) fiber	Case 1 +HT fiber
Case 4	Fluid type: crosslinked, sand type: 100 mesh_LWP+40/70_LWP	All sand replaced by light weight ones (LWP)
Case 5	Fluid type: crosslinked, sand type: 100 mesh_LWP+70% 40/70 sand + 30% 40/70_LWP	~ 30% of 40/70 sand is replaced by the LWP
Case 6	Fluid type: crosslinked, sand type: 100 mesh_LWP+37% 40/70 sand + 63% 40/70_LWP	~ 63% of 40/70 sand is replaced by the LWP
Case 7	Fluid type: crosslinked, sand type: 100 mesh_LWP+(70% 40/70 sand + HT fiber) + 30% 40/70_LWP	Case 5 + low concentration if HT fiber
Case 8	Fluid type: crosslinked, sand type: 100 mesh_LWP+(70% 40/70 sand + HT fiber) + 30% 40/70_LWP	Case 5 + high concentration if HT fiber
Case 9	Fluid type: crosslinked, sand type: 100 mesh_LWP+(37% 40/70 sand + HT fiber) + 63% 40/70_LWP	Case 6 + low concentration if HT fiber
Case 10	Fluid type: crosslinked, sand type: 100 mesh_LWP+ (37% 40/70 sand +HT fiber) + 63% 40/70_LWP	Case 6 + high concentration if HT fiber
Base case 2	Fluid type: low viscous, sand type: 100 mesh + 40/70	Base case 1 with replaced fluid
Case 11	Fluid type: low viscous, sand type: 100 mesh_LWP+70% 40/70 sand + 30% 40/70_LWP	~ 30% of 40/70 sand is replaced by the LWP
Case 12	Fluid type: low viscous, sand type: 100 mesh_LWP+(70% 40/70 sand + HT fiber) + 30% 40/70_LWP	Case 11 + low concentration if HT fiber
Case 13	Fluid type: low viscous, sand type: 100 mesh_LWP+(70% 40/70 sand + HT fiber) + 30% 40/70_LWP	Case 11 + high concentration if HT fiber
Case 14	Fluid type: low viscous, sand type: 100 mesh_LWP+37% 40/70 sand + 63% 40/70_LWP	~ 63% of 40/70 sand is replaced by the LWP
Case 15	Fluid type: low viscous, sand type: 100 mesh_LWP+(37% 40/70 sand + HT fiber) + 63% 40/70_LWP	Case 14 + low concentration if HT fiber
Case 16	Fluid type: low viscous, sand type: 100 mesh_LWP+ (37% 40/70 sand +HT fiber) + 63% 40/70_LWP	Case 14 + high concentration if HT fiber